APPLIED SCIENCES AND ENGINEERING

Sweat-sensitive adaptive warm clothing

Xiaofeng Jiang[1]†, Xiuqiang Li[1]†*, Hongbo Zhang[1], Zhili Hu[1], Siyuan Jia[1], Guowen Meng[2], Po-Chun Hsu[3], Wanlin Guo[1]*, Zhuhua Zhang[1]*

Thermal regulation in warm clothing is essential for enhancing human comfort in cold environments. However, traditional warm clothing lacks the ability to adapt to dynamic changes in the human body's microenvironment. Here, we present an adaptive warm cloth, featuring a filling made of a natural bacterial cellulose membrane that responds to human sweating. The cloth's thickness automatically adjusts from 13 millimeters (under low humidity and no sweating conditions) to 2 millimeters (under high humidity and sweating conditions), expanding the thermal regulation capability by 82.8% compared to traditional warm clothing with an unchanged thickness of 13 millimeters. Modeling results further suggest that deploying this adaptive warm clothing across 20 cities in China could extend the duration of the no thermal stress zone by an average of 7.5 hours. Combining exceptional thermal regulation, high stability, and scalability, this clothing represents a notable supplement to existing thermal management technologies.

INTRODUCTION

After a prolonged evolution process, human body has developed intrinsic mechanisms to maintain the body temperature within the normal range through the regulation of muscular activity, blood circulation, metabolic rate, as well as sweat gland function (*1*–*3*). Despite these natural adaptations, modern life often requires the use of warm clothes for thermal comfort. However, traditional warm clothes lack intelligent adaptability needed for responding to unforeseen changes in ambient temperature or metabolic heat rates (*4*–*6*). This limitation increases the risk of heat-related health issues, such as heat cramps, heat exhaustion, and neurological disorders (*7*–*9*), particularly for individuals in occupations like couriers, sanitation workers, and traffic police, who often cannot change their clothes freely. As a result, there is a growing need for the development of self-adapting warm clothing, which not only can improve personal comfort but also holds the potential to reduce energy consumption associated with air conditioning systems (*10*–*15*), offering benefits for both individuals and the environment.

To date, various strategies have been proposed to create self-adapting clothes, including modifications to textile emissivity (*16*–*18*) and porosity (*19*–*22*). While these strategies proved effective in regulating heat flux for cooling cloths, they cannot be applied to warm clothing, such as down jackets, which inherently exhibit low heat flux due to their high thermal resistance. A promising solution lies in modulating the heat conductivity of warm clothing by adjusting its thickness. Several studies have explored temperature-driven thickness-changing clothes to dynamically regulate heat transfer (*23*, *24*), which, however, primarily responds to external environmental temperature changes and exhibits limited sensitivity to changes in metabolic heat rates. In contrast, sweat response provides a more straightforward and timely reflection of the body's heat dissipation needs. Therefore, it is imperative to develop an innovative strategy for achieving sweat-responsive adaptive clothes to enable more effective thermal regulation.

Herein, we developed sweat-sensitive adaptive warm clothing (SAWC) with a unique filling composed of a passive layer and a bacterial cellulose (BC) layer responsive to sweat-induced moisture. Unlike conventional hygroscopic materials that bend when exposed to moisture, such a filling is curled in its naturally occurring state but flattens as the moisture level rises. Thus, under the sweating state, the SAWC uniquely reduces its thickness to enhance heat dissipation in response to increased microenvironmental moisture. This mechanism substantially extends both the thermal regulation capability and time, establishing an effective thermal management strategy for warm clothing.

RESULTS

As shown in Fig. 1A, the structure of our SAWC is similar to that of down jacket, but the down wool is replaced with moisture-responsive membranes. The membrane is made of a soft active layer and a rigid passive layer. In a dry environment, the length L of the bare side of the active layer decreases upon water desorption, forming a strain gradient across the membrane that drives it to bend. The bent membrane can hold up the textile to increase air presence in the SAWC, enhancing the thermal resistance for improved heat preservation (*25*–*27*). Conversely, in a humid (sweating) environment, the active layer is swelled upon water adsorption, driving the membrane to lift the bending. As a result, the membrane flattens to thin the textile for efficient heat dissipation (fig. S1). Our thermal circuit analysis (*28*) shows that the heat flux increases from 22.23 to 73.78 W/m^2 as the thickness h of the SAWC decreases from 13 to 2 mm (Fig. 1B, note S1, and fig. S2), demonstrating the unique capability of regulating heat transfer for warm clothing.

Note that existing hygroscopic materials [e.g., Nylon (*22*), Mxene (*29*, *30*), graphene (*31*–*33*), covalent organic framework (*34*), metal-organic framework (*35*), and Nafion (*36*)] commonly bend because of swelling in response to increased environmental moisture (Fig. 1C). Thus, none of these materials can be used for the design of SAWC. We selected natural BC as the active layer because it exhibits superior

[1]Key Laboratory for Intelligent Nano Materials and Devices of Ministry of Education, State Key Laboratory of Mechanics and Control for Aerospace Structures, and International Institute for Frontier Science, Nanjing University of Aeronautics and Astronautics, Nanjing 210016, China. [2]Key Laboratory of Materials Physics and Anhui Key Laboratory of Nanomaterials and Nanotechnology, Institute of Solid State Physics, Hefei Institutes of Physical Science, Chinese Academy of Sciences, Hefei 230031, China. [3]Pritzker School of Molecular Engineering, University of Chicago, Chicago, IL 60637, USA.
*Corresponding author. Email: xiuqiang.li@nuaa.edu.cn (X.L.); chuwazhang@nuaa.edu.cn (Z.Z.); wlguo@nuaa.edu.cn (W.G.)
†These authors contributed equally to this work.

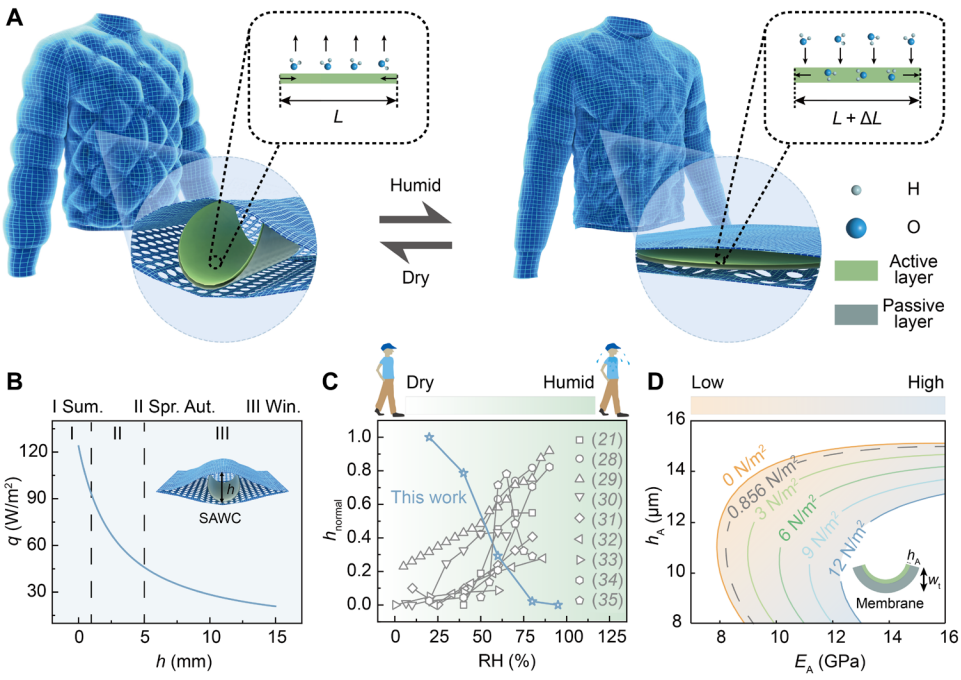

Fig. 1. Concept and mechanism of the SAWC. (**A**) Working rationale of the SAWC. (**B**) Heat flux q of the SAWC as function of thickness h; h is defined in the inset. The regions I to III represent the summer (Sum.; left), spring and autumn (Spr. Aut.; middle), and winter textiles (Win; right), respectively. (**C**) A comparison of normalized thickness (h_{normal}) between our membranes and reported hygroscopic materials under different relative humidity (RH). The background color from white to green represents the environmental state from dry to humid. The normalization is based on h of our membrane at a relative humidity of 20%. (**D**) Optimization of material parameters of the membrane by modeling. E_A, the elastic modulus of the active layer; h_A, the thickness of the active layer; and w_t, the residual thickness of the membrane, as defined in the inset. The dashed line marks the threshold force required to support the textile.

hydrophilicity resulting from abundant oxygen-containing functional groups (fig. S3). The BC layer allows for large-scale fabrication with cost-effective methods, such as blade coating and spraying. Moreover, the BC layer can be elongated up to 3.76% at a relative humidity of 95% (fig. S4), much larger than other hygroscopic materials such as cellulose acetate membrane (~1.3%) (*37*) and Nylon sewing thread (~0.6%) (*38*). However, the bending of BC layer alone was insufficient to withstand the squashing force exerted by the wrapped textile (fig. S5). As illustrated in Fig. 1D, combining BC with polyethylene terephthalate (PET) yields a standing force of 1.785 N/m^2, twice the minimum (~0.856 N/m^2) for supporting textiles (see calculation details in note S2 and figs. S6 and S7). We achieve the desired characteristics of BC/PET membrane that bends at low humidity and flattens at high humidity (Fig. 1C) by adjusting the surrounding humidity (fig. S8).

The membrane was fabricated using blade coating and ultraviolet curable techniques, as depicted in Fig. 2A. The well-developed production method enables mass production of the membrane (Fig. 2B). Then, the moisture-responsive performance of membranes was evaluated (Fig. 2C and fig. S9). The results demonstrate that the stable bending angle θ_s decreases with increasing thickness of BC and PET layers. The bending angle θ is defined as the angle between the membrane's final state, induced by moisture, and the horizontal direction, as shown in fig. S5. Furthermore, it was observed that BC10-PET20 (419.3°, where "10" and "20" represent membrane thicknesses of 10 and 20 μm for BC and PET, respectively) exhibited excessively large θ_s at a relative humidity of 20%, making it difficult to flatten textiles later, whereas BC10-PET40 exhibited a too small θ_s (69.72°) to hold up textiles. By contrast, the BC10-PET30 with θ_s = 191.72° is ideal. As the relative humidity increases from 20 to 95%, θ_s gradually decreases without any visible reverse bending due to the maximal elongation reached by the BC layer. This unique property effectively prevents textile thickness reversal at high humidity levels, thereby ensuring the robustness of SAWC thermal regulation.

Taking the optimized BC10-PET30 as the model system, the evolution of bending angle over time at different relative humidities was measured. When the membrane is transferred from a high-humidity (relative humidity of 95%) to a low-humidity environment (20, 40, 60, and 80%), the bending angle gradually increases to saturated values (Fig. 2D). Conversely, when the membrane is transferred from a low-humidity environment (relative humidity of 20%) to a high-humidity one (40, 60, 80, and 95%), the bending angle decreases over time to the correspondingly saturated value (fig. S10). These properties enable continuous thickness tuning in response to changes in humidity. To assess the temporal stability of this membrane, we record the stable bending angle over a duration of 12 hours at varied humidity levels ranging from 20 to 95%, demonstrating excellent durability of the membrane (Fig. 2D, right part). Moreover, this membrane also exhibits exceptional cycling stability without any change in the stable bending angle after 200 cycles (Fig. 2E). These remarkable properties render a capability of continuous and stable thickness (or thermal) tuning for the SAWC.

To evaluate device performance, we fabricated a 5 cm–by–5 cm unit and conducted a systematic optimization of the shape and size of the membrane as well as the lining structure. First, we performed theoretical analysis to optimize membrane shape (refer to note S2

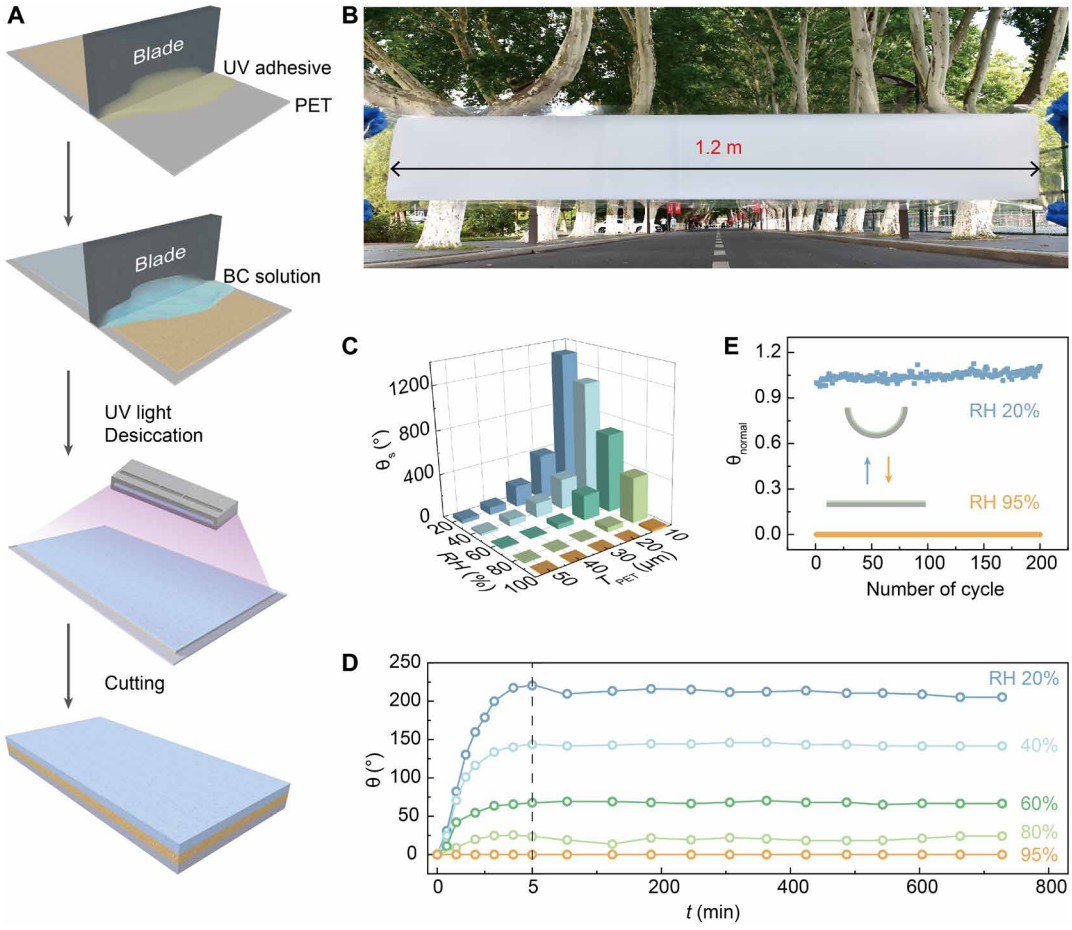

Fig. 2. Fabrication and characterization of the membrane. (**A**) The fabrication process of the membrane. UV, ultraviolet. (**B**) An image of the large-scale membrane. (**C**) A 3D plot of the membrane's stable bending angle (θ_s) versus the relative humidity and the thickness of PET. (**D**) Evolution of the bending angle (θ) of the membrane (BC10-PET30) with time at different humidity levels. The two parts separated by a vertical dashed line represent the evolution and steady stages of the bending angle, respectively. (**E**) Cycling stability of the membrane (BC10-PET30). Insets schematically illustrate membranes at a relative humidity of 20% (top) and 95% (bottom), respectively.

and fig. S6 for details). The residual thickness of the membrane within the pocket, denoted as w_t, represents the actual textile thickness under a balance with squashing from the textile. To identify the optimal shapes of membranes for maximizing the residual thickness, square, hexagon, circle, and rhombus shapes were examined by a continuum model analysis (Fig. 3A). The results revealed that, compared to other shapes, round membranes exhibited a notably larger residual thickness because it has a larger bending stiffness and experiences a smaller bending moment from textile, due to a larger width near the axis around which the membrane exhibits greater resistance to compression-induced flattening than those of hexagon and rhombus and a smaller width near the tips than square, rendering them the best choice for the SAWC design. These results are consistent with our experimental measurements shown in Fig. 3A. Second, as shown in Fig. 3B, the size of the round membrane was optimized, in terms of its diameter d ($d = 3$ or 4 cm). The result shows that the unit with a membrane of $d = 4$ cm is thicker than the one with $d = 3$ cm when swelling. Thus, $d = 4$ cm was adopted for the following study. Last, to enhance moisture-responsive time, round pores were introduced into the lining. The results demonstrate that as the pore size increases, there is a monotonic decrease in response time required for humidity change within the pocket (Fig. 3C). However, excessively large pore size or porosity leads to a decline in tensile strength (fig. S11). The lining with a moderate pore size of 5 mm in diameter was chosen.

The responsive performance of the optimized unit in various environments was measured (Fig. 3D). The results illustrate a gradual decrease in unit thickness to reach a stable value over time as the relative humidity increases from 20 to 95%. During this transition, the thickness decreases from 13.2 to 2.8 mm within 5 min (determined by reaching 95% of total transformation). Conversely, decreasing the relative humidity from 95 to 20% gradually increases the thickness back to its stable value, from 3.5 to 11.9 mm within 5 min. The unit demonstrated remarkable temporal stability across different relative humidities (Fig. 3E). In addition, after undergoing 200 cycles, the unit exhibited negligible changes in thickness at both relative humidities of 20 and 95%, indicating excellent cycling stability (Fig. 3F). The unit operates effectively across diverse environmental conditions, selectively responds to internal sweating (i.e., the humidity in the microenvironment between skin and inner side of clothes), and ensures appropriate thermal regulation across both low- and high-intensity exercise conditions for enhanced comfort

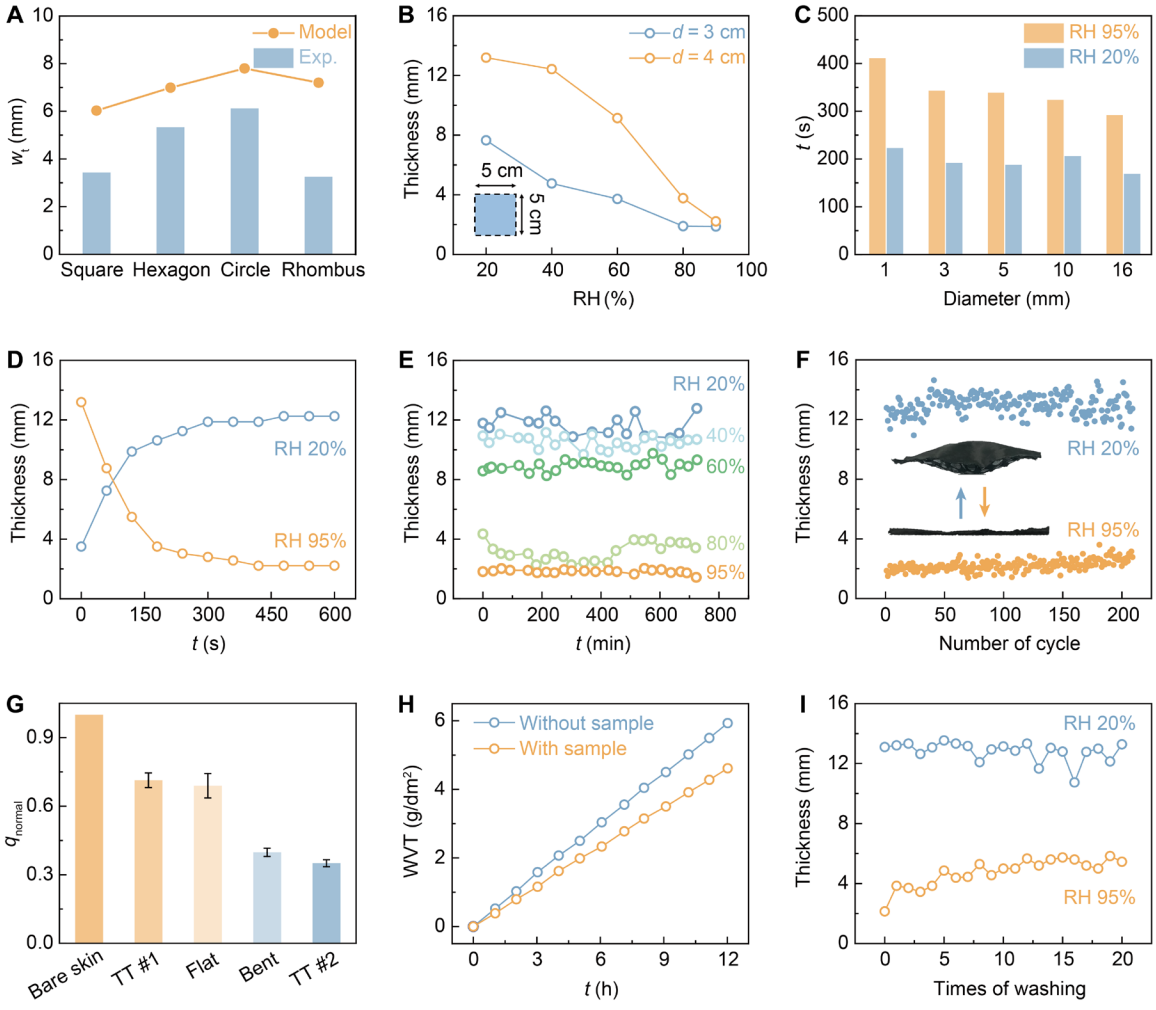

Fig. 3. Optimization and characterization of the SAWC. (**A**) The influence of the membrane's shape on its residual thickness. (**B**) Thickness of a single unit containing different round membranes (d = 3 or 4 cm) as a function of relative humidity (inset: the dimensions of the single pocket). (**C**) Effect of the size of round pores in the lining on the response time required for humidity change within the pocket. (**D**) Time-dependent thickness of a single unit containing a round membrane (d = 4 cm) under relative humidities of 20 and 95%. (**E** and **F**) The temporal (E) and cycling stability (F) of the single unit under relative humidities of 20 and 95%. Insets show a single unit under relative humidities of 20% (top) and 95% (bottom). (**G**) Normalized heat flux (q_{normal}) of different types of textiles. Traditional textile (TT) #1, commercial polyester shirt (~1.4 mm thick); traditional textile #2, commercial down coat (~13 mm thick). Error bars represent the SD of five independent measurements. (**H**) Water vapor transmittance (WVT) of the device with/without membrane. (**I**) Washing stability of the single unit. The thickness of the individual unit at different relative humidities (20 and 95%) after each washing cycle.

(figs. S12 to S16 and note S3) (*39*). The moisture responsiveness of 16 units (4 × 4 arrays) was further examined, with the configuration shown in the inset of fig. S17A. The thickness of such a large-area textile remains almost the same as that of an individual unit across different relative humidities (20, 40, 60, 80, and 95%), indicating superior integration characteristics (fig. S17). The transformation processes of individual and integrated units at relative humidities of 95 and 20% are recorded and can be compared in movies S1 and S2, respectively.

To quantify the thermal regulation capability of the SAWC, we designed and constructed a set of thermal testing equipment (*22*). The testing system features a Peltier temperature control feedback system comprised of a temperature control unit, testing unit, and data recording system (fig. S18). At a steady state, the heat flux supplied by the Peltier device is equivalent to the heating or cooling generated by simulated skin with cloth [polymer-coated copper was used to simulate human skin because they have similar emissivities; (*22*)], as measured by the heat flux sensor positioned between the Peltier device and copper plate (fig. S18, right). To ensure a fair comparison, we normalized the heat flux to 1 for bare skin. When membranes are flattened under a relative humidity of 95%, the normalized heat flux (q_{normal}) reaches 0.69 (Fig. 3G). Conversely, when membranes are bent under a relative humidity of 20%, the normalized heat flux decreases to 0.40. The normalized heat flux of traditional textiles #1 (a commercial polyester shirt, ~1.4 mm thick) and #2 (a commercial down coat, ~13 mm thick) are 0.71 and 0.35, respectively. Thus, the insulating property of the SAWC is 14.3% lower than traditional textiles #2 at low humidity. The SAWC is comparable to traditional textiles #1 in terms of heat dissipation at high humidity, but it has been enhanced by 97.1% compared to traditional textiles #2. In other words, the SAWC expands the thermal regulation

capability by up to 82.8% compared to traditional textiles #2 (see calculation details in note S4). In cold conditions (−1.3°C), the SAWC still expands the thermal regulation capability by up to 71% compared to traditional textiles #2, making it a promising material for enhanced personal thermoregulation in cold climates (fig. S19). The expansion of the thermal regulation capability relative to the traditional textiles #1 also reaches 38%. Temperature-related tests further demonstrate that the SAWC maintains stable body temperature by adapting robustly to varying sweating intensities (fig. S20 and note S5). Moreover, the presence of membranes does not notably affect the water vapor transmission of the textile (Fig. 3H). Washing test was also conducted, and each cycle involved a 30-min wash in water. There is no noticeable decline in performance even after 20 cycles (Fig. 3I).

As a demo of application, we also fabricated the SAWC by integrating membranes with a commercial down jacket to investigate its outdoor performance. The SAWCs in dry and humid states are presented in Fig. 4A [A (left) and B (left), respectively]. The fifth strip (marked "5") was left empty, while the sixth strip (marked "6") contained normal down feathers, whereas all other strips were filled with our membranes. The thicknesses of the fifth and sixth strips remain unchanged regardless of the microenvironment, while the thicknesses of other strips (filled with our membranes) decrease when changed from a dry state to a humid state. Furthermore, we evaluated the response performance of the SAWC during walking and cycling activities. The thickness of the SAWC and q_{normal} values for both walking (dry) and cycling (humid) states are recorded in Fig. 4 (C and D, respectively). Compared to walking, cycling with membranes results in a notable decrease in strip thickness and an increase in q_{normal}, indicating the autonomous regulation of human body heat by the SAWC for various real-world scenarios.

Benefiting from the exceptional heat control performance of SAWC, the outdoor workers can effectively maintain thermal comfort during various activities. To assess the impact of SAWC on outdoor workers, we used the RayMan model to calculate the predicted mean vote (PMV) thermal indexes by inputting meteorological data (air temperature, relative humidity, wind velocity, and global radiation), personal data (height, weight, age, and sex), clothing, and activity. These parameters collectively characterize the perception of thermal conditions and grade physiological stress levels. Detailed calculations are provided in note S6.

Based on the physiological stress grades, the PMV scale, ranging from −1.5 to 1.5, categorizes thermal stress as follows: −1.5 to −0.5 indicates slight cold stress, −0.5 to 0.5 represents no thermal stress, and 0.5 to 1.5 denotes slight heat stress. These ranges define suitable comfort zones for outdoor work (*40*, *41*). The comfort time is the cumulative duration within these three zones. For example, we conducted research on the comfort duration of sanitation workers wearing warm clothing and our self-adjusting wearable cooling devices on different dates in Nanjing, China. The results showed that SAWC increased their average comfort duration by ~7.1 hours and even up to 13 hours on 1 February 2024 (Fig. 5A). Moreover, SAWC has proven beneficial for various urban occupations including couriers, green workers, electricians, welders, and traffic police (Fig. 5B). While both warm clothing and SAWC provide a 24-hour comfort duration for workers (welders and traffic police, 1 January 2024), SAWC notably extend the no thermal stress zone by an average of about 4.7 hours. In a comprehensive study across 20 cities spanning four climate regions in China, SAWC exhibited remarkable heat control performance by effectively expanding the no thermal stress zone and the overall comfort zone (Fig. 5, C and D, left). The implementation of SAWC resulted in an average increase of 5.8 hours in comfort duration and extended the no thermal stress time by an additional average of 7.5 hours across these cities.

For workers required to remain in their uniforms, this extended period of comfort could potentially increase working hours and productivity, which, if fully used for work, could result in higher income levels (Fig. 5D right; see note S6 for detailed calculations).

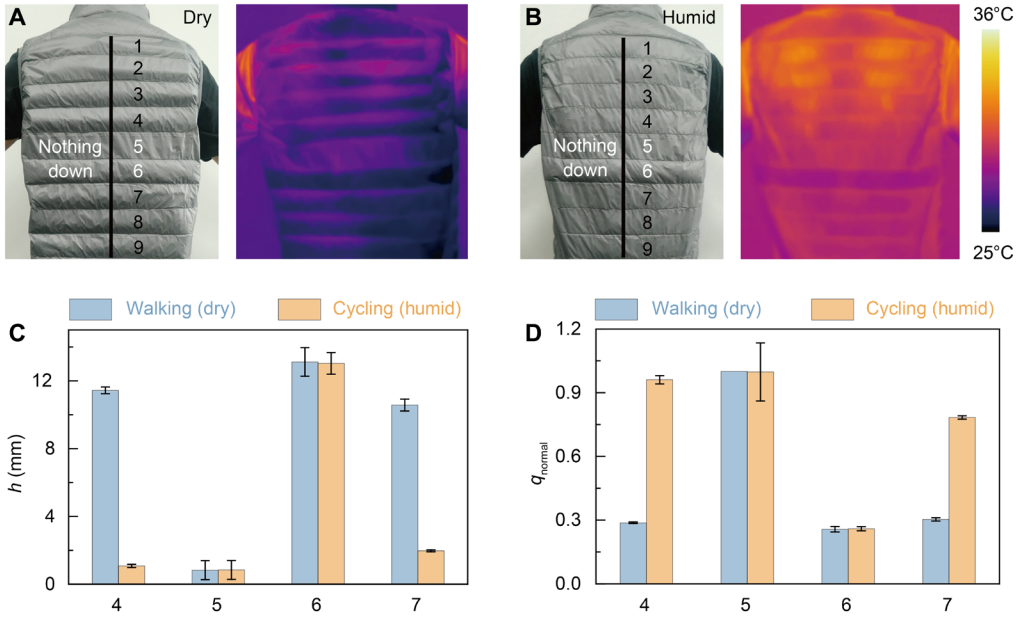

Fig. 4. Design of the SAWC and outdoor application. (**A** and **B**) Optical (left) and infrared images (right) of the SAWC in dry (A) and humid (B) states. There is nothing in the "5" pocket, but there are down feathers in the "6" pocket and membranes in all other pockets. (**C** and **D**) Thickness (C) and normalized heat flux (q_{normal}) (D) of the SAWC when walking and cycling. The normalization process is based on the heat flux of "5" in the walking state.

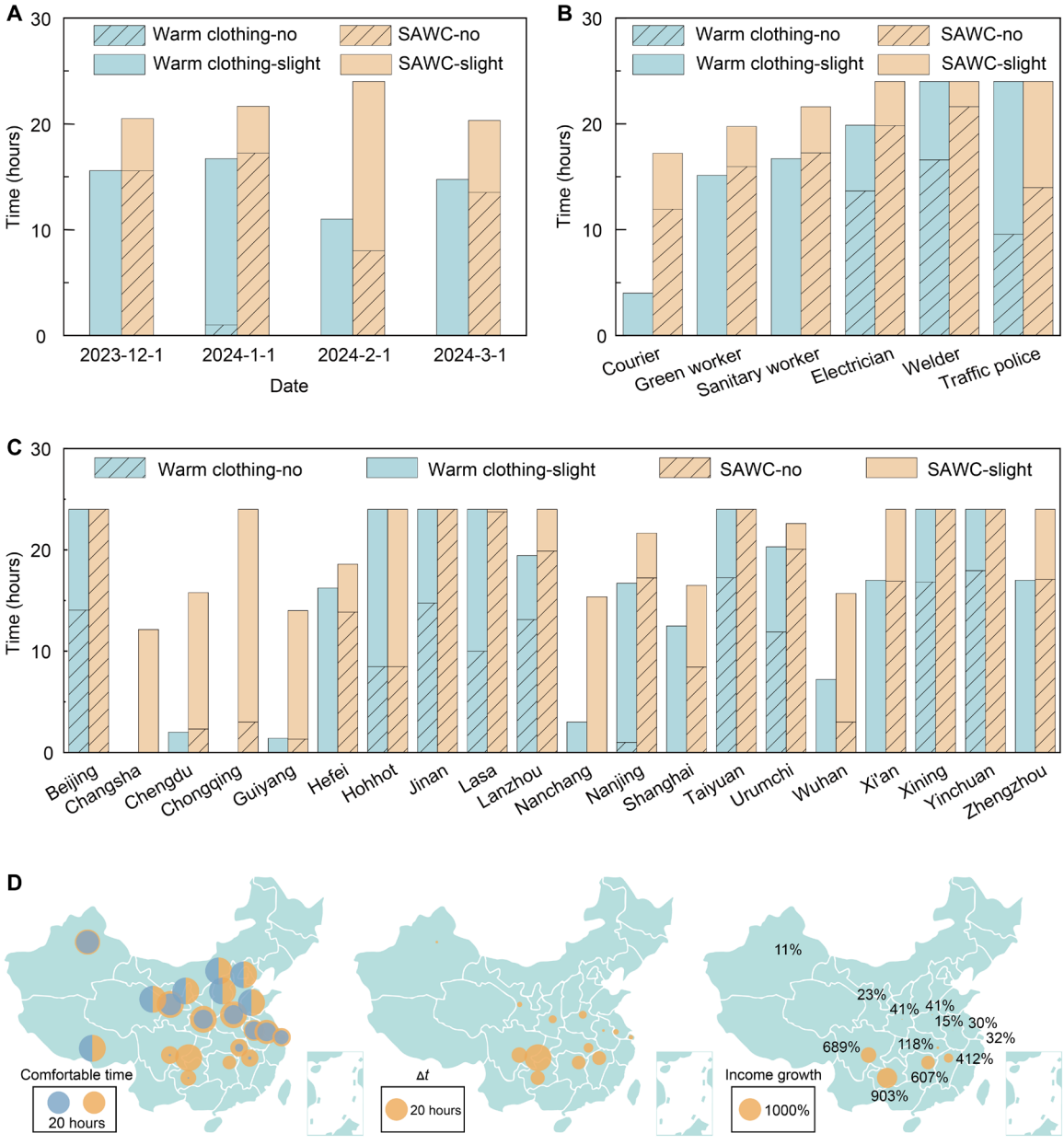

Fig. 5. Modeled comfortable time and income growth for urban outdoor workers. (**A**) The comparison of comfort time per day between sanitary workers with warm clothing and SAWC on different dates. The comfort time is the sum of the slight cold stress (−1.5 to ~−0.5), no thermal stress (−0.5 to ~0.5), and slight heat stress zone (0.5 to ~1.5). The blue (Warm clothing-no) and orange colors (SAWC-no) with patterns represent the no thermal stress zone of workers with warm clothing and SAWC, respectively. The blue (Warm clothing-slight) and orange colors (SAWC-slight) without patterns represent the sum of slight cold and heat stress zones of workers with warm clothing and SAWC, respectively. (**B**) The comparison of comfort time of different workers in Nanjing on 1 January 2024. (**C**) The comparison of comfort time for sanitary workers in different cities on 1 January 2024. (**D**) The comfort time (left), its difference (mid), and income growth (right) of sanitary workers with warm clothing and SAWCs in 20 cities in China on 1 January 2024. The blue and orange circles in the left map represent the comfort time of sanitary workers with warm clothing and SAWCs, respectively. The circles composed of a blue semicircle and an orange semicircle represent the comfort time that is 24 hours for sanitary workers with warm clothing and SAWCs. The values are scaled to the diameter of the circle.

To specifically assess SAWC's effectiveness for urban outdoor workers during working hours, we analyzed an 8-hour period from 9:00 to 17:00 and found SAWC notably extended their comfort duration (2.3 hours) for six types of work (fig. S21B). The implementation of SAWC resulted in an average increase of 1.9 hours in comfort duration and extended the no thermal stress time by an additional average of 2.6 hours across 20 cities (fig. S21C).

DISCUSSION

We have developed a scalable BC material with exceptional moisture-responsive ability and high mechanical stability. Using this material as a filling, we have fabricated a sweat-sensitive adaptive clothing that can self-adjust its thickness from 13 mm (no sweating) to 2 mm (sweating) to expand the thermal regulation capability of sweating by 82.8% compared to traditional cloth, maintaining a fixed thickness

of 13 mm. The time without thermal stress zones and comfort time are extended averagely by 7.5 and 5.8 hours, respectively, across 20 Chinese cities in four climate regions. Given the simplicity, scalability, effectiveness, and stability of the filling materials, our findings represent a promising approach for advancing personal thermal management and addressing diverse heat regulation challenges.

MATERIALS AND METHODS

Materials

PET film was purchased from Jubang (Dongguan) Plastic Raw Materials Co. Ltd. BC solution (content, 0.8%) was purchased from Guilin Qihong Technology Co. Ltd. Common textiles were purchased from Shaoxing Green Day Textile Co. Ltd. A digital humidity and temperature sensor (SEK-SHT31 Sensors) was purchased from Sensirion Co. Ltd. Deionized (DI) water (18.25 megohms·cm) was produced by a laboratory water purification system.

Fabrication of BC membrane

The PET film was washed with DI water and dried at 50°C in the oven. Then, BC solution (content, 0.8%) was coated onto the PET film by blade coating technique. The solution was dried to form a membrane in the atmosphere environment or oven. The membrane can be peeled off and cut into any expected shape.

Fabrication of membrane

PET film was washed with DI water and dried at 50°C in the oven. Then, the ultraviolet-curable adhesive and BC solution (content, 0.8%) were coated successively onto the PET film by a blade coating technique. The solution was processed for 10 min by an ultraviolet lamp and dried to form a membrane in the atmosphere or oven. The membrane can be cut into any expected shape. The BC membrane was bonded to the PET film with ultraviolet-curable adhesive at different relative humidities (20, 40, 60, 80, and 95%), which can regulate the responsive characteristics of the membrane. The membrane was processed for 10 min with an ultraviolet lamp during the preparation.

Measurements of moisture-responsive behaviors of membranes and SAWC

The humidity-controlled chambers were constructed to measure the moisture-responsive behavior (fig. S22). The digital humidity and temperature sensors (SEK-SHT31 Sensors, Sensirion Co. Ltd.) were placed in the chamber to measure humidity and temperature simultaneously. The resolution is 0.01% relative humidity and 0.01°C, respectively. The relative humidity in the chamber was adjusted by high-humidity air and drying agents. At different relative humidity, photos were taken of the membranes and SAWC using a camera positioned at the same level as the samples. Then, we used these photos to measure the bending angles of the membranes and the thicknesses of SAWC.

Water vapor transmission rate test

Glass petri dishes (6 cm in diameter) were filled with DI water and sealed with textile samples with or without membranes using rubber bands. The sealed glass petri dishes were then placed in the atmospheric environment. The total mass of the glass petri dishes together with the samples was measured periodically. The reduced mass, corresponding to the evaporated water, was then divided by the exposed area (6 cm in diameter) to derive the water vapor transmission rate.

Mechanical test

The tensile strength test was measured by ElectroForce 3200 mechanical testing machine. The BC and PET membranes were cut into the shape of 1 cm wide and 3 cm long. The fabrics with different pore sizes were cut into shapes 2 cm wide and 3 cm long. The samples were stretched until they were destroyed, and the displacement rate was kept at 4 mm min^{-1}.

Washing text

The washing tests were performed using a standard washing machine (model: [Youpin017/Ddcat]) with a power of 25 W and a capacity of 10 liters. During the tests, we used tap water without any detergent. The single pocket with membranes was washed in water for 30 min, as one wash cycle. We conducted a total of 20 cycles and measured the thickness of the sample after every cycle at relative humidity of 20 and 95%, respectively.

Thermal measurement

Figure S18 shows the schematic of thermal measurement equipment, which can quantitatively test the thermal management performance of the textile. The testing unit involves a modified copper plate, a 1-mm-thick heat flux sensor (Electro Optical Components Inc., A-04457) surrounded by glasses of equal thickness, and a proportional-integral-derivative (PID)–controlled Peltier device (TE Technology Inc., TC-36-25). Thermal grease (Dow Corning, 340) was applied to ensure good thermal contact among different parts. The testing system's sidewall is insulated with 5-cm-thick polyurethane foam to minimize heat loss. During the testing, the copper plate is kept at 34°C using the PID program to simulate the human skin temperature, while the ambient temperature is maintained at 20°C by air conditioning. At steady state, the heat flux provided by the Peltier device equals the heating or the cooling power generated by the copper plate with cloth, measured by the heat flux sensor.

Supplementary Materials

The PDF file includes:

Supplementary Notes S1 to S6
Figs. S1 to S22
Legends for movies S1 and S2

Other Supplementary Material for this manuscript includes the following:

Movies S1 and S2

REFERENCES AND NOTES

1. M. N. Cramer, D. Gagnon, O. Laitano, C. G. Crandall, Human temperature regulation under heat stress in health, disease, and injury. *Physiol. Rev.* **102**, 1907–1989 (2022).
2. C. L. Tan, Z. A. Knight, Regulation of body temperature by the nervous system. *Neuron* **98**, 31–48 (2018).
3. Y. Fang, G. Chen, M. Bick, J. Chen, Smart textiles for personalized thermoregulation. *Chem. Soc. Rev.* **50**, 9357–9374 (2021).
4. P.-C. Hsu, X. Li, Photon-engineered radiative cooling textiles. *Science* **370**, 784–785 (2020).
5. L. Lei, S. Shi, D. Wang, S. Meng, J.-G. Dai, S. Fu, J. Hu, Recent advances in thermoregulatory clothing: Materials, mechanisms, and perspectives. *ACS Nano* **17**, 1803–1830 (2023).
6. J. Yang, X. Zhang, X. Zhang, L. Wang, W. Feng, Q. Li, Beyond the visible: Bioinspired infrared adaptive materials. *Adv. Mater.* **33**, e2004754 (2021).
7. E. Pennisi, Living with heat. *Science* **370**, 778–781 (2020).
8. D. Campbell-Lendrum, T. Neville, C. Schweizer, M. Neira, Climate change and health: Three grand challenges. *Nat. Med.* **29**, 1631–1638 (2023).
9. C. Raymond, T. Matthews, R. M. Horton, The emergence of heat and humidity too severe for human tolerance. *Sci. Adv.* **6**, eaaw1838 (2020).
10. S. Shao, L. Yuan, X. Li, W. Guo, Personal thermoregulation by mid-infrared engineered materials. *Next Energy* **2**, 100083 (2024).

11. P.-C. Hsu, A. Y. Song, P. B. Catrysse, C. Liu, Y. Peng, J. Xie, S. Fan, Y. Cui, Radiative human body cooling by nanoporous polyethylene textile. *Science* **353**, 1019–1023 (2016).
12. L. Cai, A. Y. Song, P. Wu, P. C. Hsu, Y. Peng, J. Chen, C. Liu, P. B. Catrysse, Y. Liu, A. Yang, C. Zhou, C. Zhou, S. Fan, Y. Cui, Warming up human body by nanoporous metallized polyethylene textile. *Nat. Commun.* **8**, 496 (2017).
13. Y. Jing, Z. Zhao, X. Cao, Q. Sun, Y. Yuan, T. Li, Ultraflexible, cost-effective and scalable polymer-based phase change composites via chemical cross-linking for wearable thermal management. *Nat. Commun.* **14**, 8060 (2023).
14. H. Wang, Y. Zhang, X. Liang, Y. Zhang, Smart fibers and textiles for personal health management. *ACS Nano* **15**, 12497–12508 (2021).
15. Y. Zhong, F. Zhang, M. Wang, C. J. Gardner, G. Kim, Y. Liu, J. Leng, S. Jin, R. Chen, Reversible humidity sensitive clothing for personal thermoregulation. *Sci. Rep.* **7**, 44208 (2017).
16. X. A. Zhang, S. Yu, B. Xu, M. Li, Z. Peng, Y. Wang, S. Deng, X. Wu, Z. Wu, M. Ouyang, Y. Wang, Dynamic gating of infrared radiation in a textile. *Science* **363**, 619–623 (2019).
17. K. Li, C. Lin, G. Liu, G. Wang, W. Ma, M. Li, Y. Li, B. Huang, Stepless IR chromism in $Ti_3C_2T_x$ MXene tuned by interlayer water molecules. *Adv. Mater.* **36**, 2308189 (2023).
18. A. Choe, J. Yeom, Y. Kwon, Y. Lee, Y.-E. Shin, J. Kim, H. Ko, Stimuli-responsive micro/nanoporous hairy skin for adaptive thermal insulation and infrared camouflage. *Mater. Horiz.* **7**, 3258–3265 (2020).
19. W. Wang, L. Yao, C.-Y. Cheng, T. Zhang, H. Atsumi, L. Wang, G. Wang, O. Anilionyte, H. Steiner, J. Ou, K. Zhou, C. Wawrousek, K. Petrecca, A. M. Belcher, R. Karnik, X. Zhao, D. I. C. Wang, H. Ishii, Harnessing the hygroscopic and biofluorescent behaviors of genetically tractable microbial cells to design biohybrid wearables. *Sci. Adv.* **3**, e1601984 (2017).
20. J. Mu, G. Wang, H. Yan, H. Li, X. Wang, E. Gao, C. Hou, A. T. C. Pham, L. Wu, Q. Zhang, Y. Li, Z. Xu, Y. Guo, E. Reichmanis, H. Wang, M. Zhu, Molecular-channel driven actuator with considerations for multiple configurations and color switching. *Nat. Commun.* **9**, 590 (2018).
21. H. Zhao, X. Qi, Y. Ma, X. Sun, X. Liu, X. Zhang, M. Tian, L. Qu, Wearable sunlight-triggered bimorph textile actuators. *Nano Lett.* **21**, 8126–8134 (2021).
22. X. Li, B. Ma, J. Dai, C. Sui, D. Pande, D. R. Smith, L. C. Brinson, P.-C. Hsu, Metalized polyamide heterostructure as a moisture-responsive actuator for multimodal adaptive personal heat management. *Sci. Adv.* **7**, eabj7906 (2021).
23. E. Ackerman, ARPA-E energy innovation summit: Self-fluffing fabrics and the world's coolest paint. *IEEE Spectrum*, 10 March 2017; https://spectrum.ieee.org/arpae-energy-innovation-summit-selffluffing-fabrics-and-the-worlds-coolest-paint.
24. J. He, Y. Lu, L. Wang, N. Ma, On the improvement of thermal protection for temperature-responsive protective clothing incorporated with shape memory alloy. *Materials* **11**, 1932 (2018).
25. T. Xue, C. Zhu, D. Yu, X. Zhang, F. Lai, L. Zhang, C. Zhang, W. Fan, T. Liu, Fast and scalable production of crosslinked polyimide aerogel fibers for ultrathin thermoregulating clothes. *Nat. Commun.* **14**, 8378 (2023).
26. Y. Si, X. Wang, L. Dou, J. Yu, B. Ding, Ultralight and fire-resistant ceramic nanofibrous aerogels with temperature-invariant superelasticity. *Sci. Adv.* **4**, eaas8925 (2018).
27. M. Wu, Z. Shao, N. Zhao, R. Zhang, G. Yuan, L. Tian, Z. Zhang, W. Gao, H. Bai, Biomimetic, knittable aerogel fiber for thermal insulation textile. *Science* **382**, 1379–1383 (2023).
28. P. C. Hsu, C. Liu, A. Y. Song, Z. Zhang, Y. Peng, J. Xie, K. Liu, C. L. Wu, P. B. Catrysse, L. Cai, S. Zhai, A. Majumdar, S. Fan, Y. Cui, A dual-mode textile for human body radiative heating and cooling. *Sci. Adv.* **3**, e1700895 (2017).
29. J. Wang, Y. Liu, Z. Cheng, Z. Xie, L. Yin, W. Wang, Y. Song, H. Zhang, Y. Wang, Z. Fan, Highly conductive MXene film actuator based on moisture gradients. *Angew. Chem. Int. Ed.* **59**, 14029–14033 (2020).
30. G. Cai, J.-H. Ciou, Y. Liu, Y. Jiang, P. S. Lee, Leaf-inspired multiresponsive MXene-based actuator for programmable smart devices. *Sci. Adv.* **5**, eaaw7956 (2019).
31. Y. Jiang, C. Hu, H. Cheng, C. Li, T. Xu, Y. Zhao, H. Shao, L. Qu, Spontaneous, straightforward fabrication of partially reduced graphene oxide-polypyrrole composite films for versatile actuators. *ACS Nano* **10**, 4735–4741 (2016).
32. H. Cheng, J. Liu, Y. Zhao, C. Hu, Z. Zhang, N. Chen, L. Jiang, L. Qu, Graphene fibers with predetermined deformation as moisture-triggered actuators and robots. *Angew. Chem. Int. Ed. Engl.* **52**, 10482–10486 (2013).
33. D. D. Han, Y. L. Zhang, H. B. Jiang, H. Xia, J. Feng, Q. D. Chen, H. L. Xu, H. B. Sun, Moisture-responsive graphene paper prepared by self-controlled photoreduction. *Adv. Mater.* **27**, 332–338 (2015).
34. T. Mao, Z. Liu, X. Guo, Z. Wang, J. Liu, T. Wang, S. Geng, Y. Chen, P. Cheng, Z. Zhang, Engineering covalent organic frameworks with polyethylene glycol as self-sustained humidity-responsive actuators. *Angew. Chem. Int. Ed. Engl.* **62**, e202216318 (2023).
35. J. Troyano, A. Carne-Sanchez, D. Maspoch, Programmable self-assembling 3D architectures generated by patterning of swellable MOF-based composite films. *Adv. Mater.* **31**, e1808235 (2019).
36. L. Chang, D. Wang, Z. Huang, C. Wang, J. Torop, B. Li, Y. Wang, Y. Hu, A. Aabloo, A versatile ionomer-based soft actuator with multi-stimulus responses, self-sustainable locomotion, and photoelectric conversion. *Adv. Funct. Mater.* **33**, 2212341 (2022).
37. S. Khoshtinat, V. Carvelli, C. Marano, Characterization and modeling the hygroscopic behavior of cellulose acetate membranes. *Cellul.* **29**, 2175–2186 (2022).
38. J. Lee, Y. Park, Systematic investigation on the mechanisms for water responsive actuation using commercial sewing threads. *J. Nat. Fibers* **20**, 2178584 (2023).
39. W. Zhang, X. Qian, J. Fan, Y. Shi, L. Niu, Research progress on sweating rate distribution of human body. *J. Text. Res.* **39**, 179–184 (2018).
40. M. Taleghani, L. Kleerekoper, M. Tenpierik, A. van den Dobbelsteen, Outdoor thermal comfort within five different urban forms in the Netherlands. *Build. Environ.* **83**, 65–78 (2015).
41. A. M. H. Mayer, M. G. Iziomon, Applications of a universal thermal index: Physiological equivalent temperature. *Int. J. Biometeorol.* **43**, 76–84 (1999).

Acknowledgments

Funding: This work was supported by the National Natural Science Foundation of China (5230130227, 12225205, 12261160367, and U2441272), Fundamental Research Funds for the Central Universities (NS2023060), Research Fund of State Key Laboratory of Mechanics and Control for Aerospace Structures (MCAS-I-0525K01, MCAS-IS-0124K01), Key Research and Development Program of Jiangsu Province (BE2023815, BK20243044), NUAA (Nanjing University of Aeronautics and Astronautics) Startup Fund (4017-YQR22012), and Jiangsu Specially-Appointed Professors. **Author contributions:** Conceptualization: X.L., W.G., and Z.Z. Investigation: X.L., X.J., and S.J. Methodology: X.L., Z.Z., X.J., and S.J. Visualization: X.J., H.Z., and S.J. Supervision: X.L., W.G., and Z.Z. Software: X.J., H.Z., and Z.H. Project administration: X.L., W.G., and Z.Z. Writing—original draft: X.L., W.G., Z.Z., X.J., and Z.H. Writing—review and editing: X.L., W.G., Z.Z., X.J., H.Z., Z.H., S.J., G.M., and P.-C.H. **Competing interests:** X.L., X.J., Z.Z., and W.G. are inventors on two patent applications (application nos. CN202311015818.6 and CN202311015819.0) related to this work. The name of the organization filing the patents is Nanjing University of Aeronautics and Astronautics. All other authors declare that they have no competing interests. **Data and materials availability:** All data needed to evaluate the conclusions in the paper are present in the paper and/or the Supplementary Materials.

Submitted 3 November 2024
Accepted 14 July 2025
Published 13 August 2025
10.1126/sciadv.adu3472